Fall of Parp3 restrains Lgr5+ stem cells proliferation and mucosal renovation in intestinal aging

Xiuying Peng (pengxy29@mail2.sysu.edu.cn)
Third Affiliated Hospital of Sun Yat-Sen University https://orcid.org/0000-0001-5308-0110

Huiling Liu
Third Affiliated Hospital of Sun Yat-Sen University

Jiancheng Wang
The Seventh Affiliated Hospital Sun Yat-sen University

Jie Jiang
Third Affiliated Hospital of Sun Yat-Sen University

Hainan Chen
Sun Yat-Sen University

Jin Tao
Third Affiliated Hospital of Sun Yat-Sen University

Bin Wu
Third Affiliated Hospital of Sun Yat-Sen University

Research Article

Keywords: Aging, Intestine, Lgr5+ISCs, Parp3

Posted Date: February 24th, 2022

DOI: https://doi.org/10.21203/rs.3.rs-1317329/v1

Abstract

Background

The aging small intestine has a great impact on body health. One of the obvious characteristics is the degeneration of epithelium turnover. The acknowledged $Lgr5^{+}$ intestinal stem cell is the key factor.

Methods

We used Lgr5-EGFP transgenic mice in three different ages (young group:3-6 months, middle group:12-14 months and old group:22-24 months) to mark the $Lgr5^{+}$ISCs. We collected the jejunum for histology, immunofluorescence, western-blotting and PCR, we isolated the crypts for organoid culture and sorted out the $Lgr5^{hi}$ cells for bulk RNA sequence.

Results

In tissue, the crypts depth, proliferating cells and $Lgr5^{+}$ISCs number increased in middle group (12-14 months) and then decreased in old group (22-24 months). The number of proliferating $Lgr5^{+}$ISCs gradually decreased from young to old. In organoids, the buddings number and projected area, $Lgr5^{+}$ISCs ratio also decreased from young to old. Both gene expression of *Parp3* and protein level of Parp3 increased in middle and old group. Parp3 inhibitors slowed down organoids' growth of the middle age.

Conclusion

Parp3 might participate in regulating the proliferation capacity of $Lgr5^{+}$ISCs during aging.

Introduction

Small intestine (SI) is an organ which performs a wide range of functions in physiological processes, including absorbing the nutrition, secretion, excretion as well as immune modulation [1]. Intestinal homeostasis depends on the close cooperation between the intestinal epithelium, the microbiota and the host immune system [2]. These factors are involved in maintaining intestinal homeostasis and their functions decline with age, leading to significant disturbances in intestinal homeostasis. As clinical researches indicated, nutrient malabsorption is prevalent among the aged, followed by anemia and other disease [3]. In addition, elderly individuals are prone to colorectal cancer, accounting for 88% of CRC patients in the United States diagnosed in 2020[4]. Other than that, complications in the intestinal system were found to increase with age, such as insulin resistance [5], obesity [6], even the overall health condition problem. In conclusion, the aging small intestine shows decreasing ability of absorption, microbiota dysbiosis, increasing inflammatory response, and more susceptibility to infection and tumor

[7]. As mentioned above, intestinal homeostasis is of significance for its functionality and maintenance of the epithelial barrier, without which health problems occur. Therefore, the study concerning aging intestine appears vital in particular.

With a characteristic of rapidly self-renewing every 4-5 days [8], the small intestinal epithelium plays a leading role in SI function and intestinal homeostasis. The continuous regeneration of the intestinal epithelium highlights the vital role of intestinal stem cells (ISCs) in human body. ISCs, which express markers such as Lgr5, are located at the bottom of crypts and perform persistent cell divisions to renovate the intestinal epithelium during our whole life [9]. Previous studies showed that there was a decline in the regeneration capacity of ISCs from the old mice compared to the young [10]. With the aging-related changes in ISCs, structural differences were observed in old intestine crypts that there was an increment in crypt length and width for the increase of cells in crypt, while the number of crypts had a reduction [10]. Moreover, ISC dysfunction correlated with senescence was also seen in vitro organoids forming that there was a significant reduction in the number of organoids derived by crypts from old mice and aged human [11]. These self-renewal and epithelium-forming hypofunctions in senescent ISCs also declines the repair ability of the intestinal epithelium when ROS or short telomeres leads to DNA damage [12, 13, 14]. Overall, senescent ISCs exert pressure for a constantly renewing epithelium as well as its protective function, followed by intestinal homeostasis disorder and age-related diseases.

There are plenty of hypotheses that explain the senescence mechanism of ISCs, however, the decline of Wnt signaling pathway seems to play a central role [15]. Under normal circumstances, the nutrition and protection of Paneth cells can maintain the homeostasis of ISCs [16], while aged Paneth cells may produce Notum, an extracellular Wnt inhibitor, which caused a decrease of Wnt signaling in ISCs [11]. The decline of canonical Wnt signaling in ISCs would eventually lead to the senescence of ISCs and reduction in regenerative capacity [17]. Moreover, ROS accumulation and autophagy system malfunction also contribute to ISC senescence process [18, 19]. Previous article showed that ROS accumulation in aging ISCs led to mitochondrial dysfunction and damage of DNA and protein [20]. And impaired autophagy-related pathway disturbed the clearance and recycling of DNA and protein in ISCs [21]. In general, decline of Wnt signaling, ROS accumulation and autophagy malfunction affect ISC senescence together. However, the molecular mechanism of ISC senescence has not been elucidated, especially the special mechanism that distinguishes it from other adult stem cells.

In this study, we divided the mice in three groups according to different age: the young group (3-6 months), the middle group (12-14 months) and the old group (22-24months). Since we wanted to explore the whole process of aging in small intestine, we added the middle group as transition between the youngand old group. We used immunofluorescence, crypt isolation, organoids culture and RNA sequence to explore the $Lgr5^+$ ISCs in different groups. We found that the proliferation capacity of $Lgr5^+$ ISCs decreased during aging and Parp3 protein may participate in regulating the proliferating function.

Material And Methods

Ethics approval and Animals

The animal use and experiments were approved by the Ethics Committee of Third Affiliated Hospital of Sun Yat-Sen University. Mouse lines used: C57BL/6 mice, Lgr5-EGFP mice (Jackson lab, America). All the C57BL/6 mice were housed in Animal Centre of the Third Affiliated hospital, Sun Yat-Sen University. The ISC marker leucine-rich repeat- containing G protein-coupled receptor 5 knock-in mice (Lgr5-EGFP mice) was purchased from Jackson lab and breed on the Animal Centre. The mice were housed in microisolator cages with unrestricted water and ad libitum. The 3-6 months mice were in the young group, the 12-14 months mice were in the middle group and the 22-24 months mice were in the old group. Each group of mice were intraperitoneal injected BrdU (Abcam, America) solution (1mg/10g, 10mg/ml in normal saline). After 72 hours, the mice were sacrificed and taken the small intestine sample.

Intestinal crypt isolation

In brief, the section of the initial part of the small intestine was opened lengthwise, cleaned with cold PBS 5-10 times and, after removal of villi by scraping with a cold glass slide, sliced into small fragments roughly 2mm in length. The tissue was then incubated in 5mM EDTA/PBS at 4°C for 30 min with shaking. Supernatant was removed and pieces of intestine were re-suspended in DMEM/F12 (Gibco, America) with 0.1% BSA. The tissue was then shaken vigorously. To collect the first fraction, the suspension was passed through a 100μm strainer. The remaining tissue pieces were collected from the strainer and fresh DMEM/F12 (Gibco, America) with 0.1% BSA was added, followed by vigorous shaking. The crypt fraction was again collected by passing through a 100μm strainer. In total, 4 fractions were collected. Each fraction was centrifuged at 300g for 5 min at 4°C. Supernatant was removed and this procedure was repeated three times to purify the crypts.

Organoid culture and passage

The crypts were counted under light microscope and the suspension with calculated volume was taken to another tube. The suspension was centrifuged at 300g 5min to gain the precipitate. The precipitate was resuspended with DMEM/F12 (Gibco, America) and mixed well. The suspension was centrifuged at 300g 5min to discard the supernatant. The crypts were mixed with Matrigel (Growth Factor Reduced, Corning, America) in 1000/100μl by precooled pipette in ice box. The mixture was planted on a 24-holes plate preheated in Cell incubator (37°C,5%CO_2) with 50μl a hole. Then the plate was put into cell incubator for 20 min to make Matrigel (Growth Factor Reduced, Corning, America) solidify. Then the IntestiCult^{TM} Organoid Growth Medium (Mouse) (STEMCELL Technologies, Canada) was added in each hole. The culture medium was changed twice in one week.

When the organoids cultured after 7-10 days, they could be passaged. The culture medium was moved and GDCR (STEMCELL Technologies, Canada) was added. The liquid and Matrigel (Growth Factor Reduced, Corning, America) was blown by fluid gun and collected in a tube. The tube was shaken 20 min and centrifuged at 300g 5min. The precipitate was resuspended with DMEM/F12 (Gibco, America) and mixed well. The suspension was centrifuged at 300g 5min to discard the supernatant. The precipitate

was mixed with Matrigel (Growth Factor Reduced, Corning, America) and plated into the plate as above mentioned. The organoids used for this article were no more than 2 passage.

The organoids were observed under a microscope (Axio Observer 3, Carl Zeiss) or Operetta CLS^{TM} high-content analysis system (PerkinElmer).

Histological analysis

Paraffin-embedded jejunums were cut into 3μm thick section. The sections were used for hematoxylin and eosin (Leagene, China) staining for histological analysis. And the sections were used for Alcian-blue and Periodic Acid-Schiff (Leagene, China) staining to count the goblet cells.

Immunohistochemistry and immunofluorescence

For immunohistochemistry, the paraffin sections were deparaffinized and rehydrated. The section was soaked into 3%H_2O_2 solution 10min and then into boiled pH6.0 citrate sodium 3 min for antigen retrieval. The blocking buffer was used on section for 15min to bind the non-specific antibody. The section was washed by PBST buffer. Then the section was incubated with primary antibody (MMP7, anti-rabbit, 1:400, Cell Signaling Technology, America; PCNA, anti-rabbit, 1:200, Cell Signaling Technology, America) at 4°C overnight and then with a secondary antibody at 37°C for 120 min. The signal was detected with a diaminobenzidine kit (Leagene, China) and the nuclear was stained by hematoxylin.

For immunofluorescence, the paraffin sections were treated as mentioned above before incubated secondary antibody. The sections were incubated with secondary antibody at 37°C for 90min. Then the sections were stained with DAPI for nuclear marker. The frozen sections were fixed with 4% paraformaldehyde at 15min, permeated with 0.5% Triton 20min, and then incubated with the blocking buffer 15min. The section was incubated with primary antibody (Olfm4, anti-rabbit, 1:400, Cell Signaling Technology, America; BrdU, 1:100, Abcam, America; GFP, anti-rabbit, 1:200, ABclonal, China; GFP, anti-mouse, 1:100, ABclonal, China; Ki67, anti-rabbit, 1:200, Abcam, America;Parp3, anti-rabbit, 1:100, Invitrogen, America) at room temperature for 120 min and then with a species-appropriate secondary antibody (Alexa Fluor^{TM}488, anti-rabbit; Alexa Fluor^{TM}488, anti-mouse; Alexa Fluor^{TM}488, anti-mouse; Alexa Fluor^{TM}594, anti-rabbit, 1:400, Thermo Fisher SCIENTIFIC, America) at 120 min. The sections were stained with DAPI for nuclear marker. The stained sections were then scanned using a microscope (DM4000, Leica) or a confocal microscope (LSM880, Carl Zeiss) in single-photon mode with an appropriate wavelength depending on the primary antibody and the presence of endogenous fluorophores.

Total RNA extraction and real-time PCR

Total RNA was extracted from the intestinal mucosa scraping samples using Tissue RNA Extraction Kit according to the manufacturer's instruction. RNA was reversed transcription to cDNA with Kit (ReverTra Acetm qPCR RT Master Mix) according to the manufacturer's instruction. Real-time PCR was performed on an ABI7500 using gene-specific primers and SYBR Mix. Each reaction consisted of 2μL of cDNA

product, 2.5μM of primers and 7.2μl of SYBR® Green real-time PCR master mix. The reactions were incubated in a 96-well plate at 95°C for 5 min, followed by 45 cycles of 95°C for 15s, 60°C for 20s and 72°C for 40s. After the reactions were completed, the threshold was manually set and the threshold cycle (CT) was automatically recorded. The CT is defined as the fractional cycle number at which the fluorescence signal passes the fixed threshold. All reactions were run in three replicates for each sample.

The comparative CT method was used to calculate the expression relative to the endogenous control.

(*Parp3*: Forward primer: ATGGCTCCAAAACGAAAGGC, Reverse primer: TCCTCCTCTGTCCCTTGTCG;

Actin: Forward primer: CGTGCGTGACATCAAAGAGAA, Reverse primer: CCAAGAAGGAAGGCTGGAAAA)

Protein extraction and western-blotting analysis

Tissue was homogenised in PBS using an electrical homogeniser and protein extracted in the presence of protease inhibitors (in 325μl PBS, 25μl aprotinin (2.2mg/ml), 25μl trypsin inhibitor (5mg/ml), 25μl 10% Nonidet, 25μl sterile water) on ice with periodic vortexing for 30–40 min, and lysates were cleared by centrifugation at 10,000×g for 10min at 4°C, and the supernatants were used for immunoblotting following boiling in 1×SDS-sample loading buffer for 5min. Protein concentrations were determined by spectrophotometry with a BioRad protein assay (Bradfords' method) (BioRad Laboratories, Munchen, Germany). The standard curve was performed using 0, 2, 4, 8, and 16g of bovine serum albumin/ml.

For analysis samples (10–50μg protein) were separated on 8%, 10% or 12% SDS-polyacrylamide gels followed by transfer to nitrocellulose membranes (Bio-Rad) and immunoblotting with the indicated antibodies: Parp3 (1:500, anti-mouse, Santa Cruz Biotechnology, America) and β-Actin (1:2000, anti-mouse, Santa Cruz Biotechnology, America). Blots were developed with chemiluminescence and detected by ChemiDoc^{TM}Imaging System (Bio-Rad).

TUNEL staining

TUNEL staining of cells was carried out with the TUNEL Apoptosis Assay Kit (Servicebio, China) according to the manufacturer's instructions, respectively. Briefly, cells were permeabilized with freshly prepared 0.05% Triton X-100 and 0.1% sodium citrate for 15min at room temperature, and rinsed with 50μl of TUNEL reaction mixture for 6min at 37°C in the dark. Next, the cells were incubated with DAPI for 10 min. Images were captured using a fluorescence microscope (DM4000, Leica) or a confocal microscope (LSM880, Carl Zeiss).

Senescence-associated β-galactosidase staining

Senescence β-galactosidase staining of cells was carried out with the Senescence β-Galactosidase Staining Kit (Beyotime Biotech) according to the manufacturer's instructions.

Briefly, cells were washed in PBS, fixed in fixative solution (2% formaldehyde and 2% glutaraldehyde) for 15min, and stained with β-galactosidase staining solution overnight at 37°C. Images were acquired using a microscope (Axio Observer 3, Carl Zeiss).

FACS and bulk RNA-sequence

The FACScan flow cytometer (BD Biosciences, Franklin Lakes, NJ) was used to perform FACS analysis as previously described with minor modification. Crypts were digested with Tryple Express for 30min to separate into single cells. About 5×10^5 freshly FACS sorted GFP-Lgr5^{hi} cells were re-suspended in TRIzol reagent after washing with PBS. After isolated from the TRIzol lysate, the RNA samples were constructed into RNA sequencing libraries by using a NEBNext® Ultra™ RNA Library Prep Kit for Illumina® (E7530L, New England Biolabs) according to the manufacturer's instructions.

Statistical analysis

Statistical analyses were performed using SPSS version 20.0. The data collected from organoids or determined by PCR and western-blotting have been expressed as scar bar (mean ± SE). The Comparison of three groups was done by Anova. Then a Bonferroni test was used to compare each two groups. $P<0.05$ means significant difference between two groups. The data collected from tissue or the single organoid in different ages have been expressed as box plot. The comparison of three groups was done by Kruskal-Wallis text. $P<0.017$ means significant difference between two groups.

Results

Intestinal villus length and crypt base columnar cells (CBCs) were reduced in aging.

To explore the morphology of intestinal epithelium in three ages mice, we used hematoxylin-eosin staining to count the villi height and crypt depths. Villi height was no difference between young and middle groups, but decreased in old group compared with young and middle groups. Crypt depth was increased in middle group compared with young group, but decreased in old group compared with middle group (Fig. 1a). To count the major kinds of epithelium, we used Alcian blue and Periodic Acid-Schiff staining, MMP-7 immunohistochemistry staining and Olfm4 immunofluorescence to mark goblet cells, Paneth cells and ISCs respectively. Goblet cells number in crypt-villi axis were no difference among three groups (Fig. 1b). Paneth cells number was increased in middle group compared with young group, and was no difference between middle group and old group (Fig. 1c). Olfm4$^+$ crypt base columnar cells (CBCs) were increased in the middle group compared with young group and then decreased in old group (Fig. 1d). Crypt depth and number of Olfm4$^+$CBCs showed similar tendency in aging. These results indicated that the number of ISCs and proliferation might be increased in middle age and decreased in old.

Lgr5 $^+$ intestinal stem cells (ISCs) were reduced in aging mice and intestinal organoids.

To verify the ISCs number in different ages, we used Lgr5-EGFP knock-in transgenic mice to mark the Lgr5$^+$ISCs. The number of Lgr5$^+$ISCs in each crypt increased in middle group and then decrease in old group (Fig. 2a), which is consistent with the number of Olfm4$^+$CBCs (Fig. 1d). Next, we isolated the crypts from Lgr5-EGFP mice in different ages and cultured organoids for 7 days to explore whether the ISCs

from different ages mice were distinguish in culture condition. In the view of single organoids, the buddings number and projected area were decreased both in middle group and old group compared with young group and were no difference between middle group and old group (Fig. 2b). In the view of holes, the Lgr5-GFP area tended to decrease in old group but had no statistical difference (P=0.067 among three groups) (Fig. 2c). In the view of sections, the ratio of $Lgr5^+$ISCs number to DAPI number decreased in old group compared with young group (Fig. 2d). These results above suggested that the number of $Lgr5^+$ISCs decreased in old mice both *in vivo* and *in vitro*.

Intestinal cellular proliferation was downregulation in aging mice and intestinal organoids.

To further verify the proliferation in aging, we used PCNA and Ki67 to mark the proliferating cells. The results showed that proliferating cells in crypts increased in middle group compared with young group, and then decreased in old group compared with middle group. The young group and old group were no difference (Fig. 3a and 3b). To explore the movement of epithelium, we intraperitoneally injected BrdU (5-bromo-2'-deoxyuridine) into mice and collected the samples after 72 hours. After BrdU immunofluorescence staining, we calculated the distance from the middle point of $BrdU^+$ cells to the bottom of villi. The result showed that the distance decreased gradually from young group to old group (Fig. 3c). To verify the proliferation in organoids, we used organoids section for Ki67 immunofluorescence. The ratio of $Ki67^+$ cells decreased in old group compared with young group (Fig. 4a). These results suggested that the proliferation decreased in old groups. In middle group, the proliferation increased only in tissue.

Proliferation of $Lgr5^+$ ISCs was restrained in aging mice.

According to the results above, we found that the number of $Lgr5^+$ ISCs and its related proliferation function changed in aging. Next, we intended to explore which status in $Lgr5^+$ ISCs caused such results, proliferation, apoptosis or cells senescence. We used Lgr5-EGFP mice to mark the $Lgr5^+$ ISCs. Meanwhile, we used Ki67 immunofluorescence to mark the proliferating $Lgr5^+$ ISCs and TUNEL to mark the apoptosis $Lgr5^+$ ISCs. The proportion of proliferating $Lgr5^+$ ISCs decreased in middle and old group compared with young group. The results of middle group and old group were no difference (Fig. 4a and 4d). Among all the three group, none of $Lgr5^+$ ISCs were TUNEL positive. Although some $TUNEL^+$ fragments were observed on the crypt basement in old group, these fragments did not overlap with nuclear or Lgr5-GFP signals (Fig. 4b).

Lastly, we used a canonical cell senescent marker-β-galactosidase staining on isolated crypts and villi, 24-hours cultured organoids and 7-days cultured organoids to detect the cell senescence. The result showed that all of the villi and the top of the crypts were blue, however, the bottom of the crypts were unstaining in all three groups, which suggested the majority of intestinal epithelium were already senescent at three months while ISCs were not. In addition, organoids from different groups were almost staining blue, while some newborn buddings were unmarked (Fig. 4c and 4d).

All the results showed that the proliferation Lgr5^{+}ISCs function degenerated obviously.

Parp3 gene was upregulated in intestinal Lgr5^{+} stem cells of aging mice.

Since we found that the proliferation of Lgr5^{+} ISCs degenerating in aging impacted the renovation of intestinal epithelium, to understand the molecular mechanism of Lgr5^{+} ISCs in different age, we isolated the crypts, separated them into single cell and sorted the Lgr5^{high} cells by FACS for bulk RNA sequence (Fig. 5a). The flow chart showed that the percentage of Lgr5^{high} cells increased in middle group and decreased in old group (Fig. 5B), which was consistent with former results (Fig. 2a). The whole heat map showed that 9 samples were divided into three clusters according to gene expression, which were consistent of the age groups (Fig. 5c). The majority of genes expression were similar between middle and old group, with only 55 genes up-regulated and 85 genes down-regulated in old group. And 211 genes upregulated and 93 genes downregulated in middle group compared with young group. Furthermore, we used the pathway enrichment to analysis the signal transduction among the three groups. For example, there were statistical differences in immune-related signaling pathways between the young and middle group such as antigen processing and presentation pathway. (Fig. 5d) Between middle group and old group, pathways such as DNA methylation and Meiotic Recombination had statistically significant difference (Fig. 5e). We noticed that the *Parp3* had significantly statistical difference in the young group compared with both middle group and old group (Fig. 5f). *Parp3* was also into the KEGG pathway “cell growth death”. We hypothesized that this gene might relate to the alternation of Lgr5^{+} ISCs proliferation in aging.

Parp3 was overexpressed in intestinal mucosa and intestinal organoids of aging mice.

To further verify the *Parp3* expression in different ages, we used RT-PCR, western-blotting and Parp3 immunofluorescence to determine the gene expression and protein expression of Parp3. *Parp3* gene expression increased in old group compared with young group and showed a tendency of increase in middle group compare with young group but had no statistical difference (Fig. 6a). Parp3 protein expression increased in middle group and old group compared with young group. And the protein expression was no difference between middle group and old group (Fig. 6b). The results of Parp3 immunofluorescence on tissue and organoids also showed Parp3 protein level increased in middle and old group (Fig. 6c and 6d). These results indicated that Parp3 gene expression and protein level increased in aging.

Inhibition of Parp3 depressed intestinal organoids growth in aging.

Since we found that the Parp3 increased from the middle age and keeping high level in the old, next, we explored the effect of Parp3 on epithelium. We cultured the organoids from 12 months Lgr5-EGFP mice. We used two kinds of Parp3 non-selective inhibitors, AZD-2461 and ME0328, with a concentration of 2μmol/L and 10μmol/L respectively. The inhibitors were added into the culture medium in day 4, and the culture medium was changed every day until day 7. We added the equally volume of DMSO in culture

fluids as control groups. We traced the organoids in these groups in day 4 and compared the organoids shape every day after adding the inhibitors. The organoids in both of AZD-2461 groups and ME0328 group grew less volume and buddings compared with control group (Fig. 7a-c). To observe the expression of Parp3, we used Parp3 immunofluorescence to detect the Parp3 protein in organoids after 7-days cultured. The results showed that Parp3 had a lower lever in the two groups adding inhibitors compared with control group (Fig. 7d). All the results showed that inhibition of Parp3 depressed the middle age organoids growth.

Discussion

We started our research with history analysis. As mentioned in the literature, the villi height and crypt depth measured in different articles varied [22]. Moreover, previous studies evaluating the number of goblet cells, Paneth cells and stem cells also observed inconsistent results [23, 24]. This discrepancy could be attributed to the following two reasons. First, the samples taken by different researchers may be situated in different parts of the small intestine, which account for different results. An article about a single cell survey of intestinal epithelium revealed that the mRNA expression from jejunum to ileum gradually changed [25]. Therefore, in our research, we used the jejunum (proximal small intestine) sample in a similar location to compare.

There is, however, another possible explanation revealed in our article--the aging process can be divided into 2 stages with different characteristics. This opinion was further verified by the results of bulk RNA sequence of Lgr5^{hi} cells. Generally speaking, compared with young age (3-6 months), mice jejuna in middle age group (12-14 months) have the following changes. According to the BrdU staining results, the turnover of intestinal epithelium in middle age slowed down but can still reach the top in the third day (72 hours after injection). However, the crypts length, the number of proliferating cells and ISCs in each crypt increased in the middle age group. The villi height can still be maintained in the middle age. These results suggested that in the middle age, proliferation enhanced to maintain the villi length. The old age (22-24 months) mice showed function drops in comparison with the middle age mice. In the old mice, the villi height decreased and renovation of intestinal epithelium obviously slowed down. The crypts depth, number of proliferating cells and ISCs in each crypt decreased as well. These results showed that in old mice, the proliferation function is severely impaired, causing the functional area to decrease. Otherwise, in all three groups of this study, the number of goblet cells in each crypt-villi axis shows no difference, which might because of the low density of goblet cells in jejunum [26]. The number of Paneth cells increased during aging, which is consistent with the findings previous articles presented [27].

Based on the result we showed above, we found the key point of intestinal epithelium homeostasis during aging is crypts. To further detect whether the crypts from different age of mice have intrinsically difference, we isolated the crypts and cultured the organoids *in vitro* [28]. Under the organoid cultured conditions, the culture conditions among three groups were same and the mechanism of other systemic homeostasis regulation was absence so that the influence of other systems such as immune system, vessel system and the mesenchyme in aging process could be excluded [29]. Although the organoids

growth is related to density of crypts, we still found that the maximum number of buddings and projected area on each organoid decreased in middle and old age, which is consistent with the previous article. [24] In addition, the result also showed that the Lgr5 expression and the proliferating cells gradually decreased from young group to old group. However, we noticed that in the cultured condition organoids from the middle groups didn't show increase on proliferation and $Lgr5^+$ISCs, which is inconsistent with the results *in vivo*. It might be related to the systemic regulation mechanism *in vivo*.

Next, we explored what led to the ISCs dysfunction and decreased, and we supposed that it was caused by cell senescence, apoptosis or proliferation. Initially, we used β-galactosidase staining to mark the senescence cells in 24-hour cultured and seven-day cultured organoids. To our surprise, the negative cells were hardly seen in all groups and the average density is no difference. Then we stained the isolated crypts and villi fragment and found that in all three groups, the basement of crypts, where the ISCs located, was negative. So, we realized that this canonical senescence marker might not suitable for ISCs. Moreover, we used the TUNEL staining to detect the level of apoptosis of ISCs. The result showed that the old ISCs had no apoptosis, but some positive fragments were observed in the old crypt basement. Finally, the proliferation is the only obvious difference. In situ, the ratio of proliferating $Lgr5^+$ISCs decreased in the middle groups and old groups, which was consistent with the buddings and projected area of organoids.

Our study showed that the regenerative capacity of $Lgr5^+$ISCs were impaired in aging intestine and the number of $Lgr5^+$ISCs changed with age. Furthermore, we isolated the $Lgr5^{hi}$cells in crypts from the three different age classes and the RNA sequence results showed that the gene expression of the cells in middle-aged group was similar to the old rather than that in the young group. It is consistent with the age-related trend in the ratio of proliferating $Lgr5^+$ISCs in situ, the buddings number and projected area of organoids *in vitro*. Then, focusing on the "cell growth and death" of KEGG second class, we identified Parp3 as a factor performing such functional role in the age-related changes of $Lgr5^+$ISCs.

Poly (ADP-ribose) polymerase 3 (Parp3) is a member of ARTD (Parp) family which can synthesize poly (ADP-ribose) at the expense of NAD^+ [30]. Previous studies showed that Parp3 was involved in the cellular response to DNA damage [31], mitotic progression [32], chromosomal rearrangements [33], the regulation of redox homeostasis [34] and tumor aggressiveness [35]. Moreover, Parp3 inhibitor ME0328 was found to cause cell cycle arrest in breast cancer cells [36]. Thus, after we respectively added two kinds of Parp3 inhibitor in the organoids derived from the middle age (12 months) mice, the organoids growth was obviously blocked. Our results suggest that increased Parp3 underlies $Lgr5^+$ISCs in aged groups to maintain the proliferation function, but the molecular mechanism is needed to be further explored. It is likely that Parp3 has similar homeostatic roles in other stem cells during aging, which is needed to be further explored.

Conclusion

In summary, we found the number and proliferation of $Lgr5^+$ISCs increased in middle age and decreased in old age. Parp3 expression increased in middle and old age. Parp3 inhibitors depressed intestinal organoids growth in middle age. Parp3 might play an important role in $Lgr5^+$ISCs regulation in aging.

Abbreviations

CBCs
crypt base columnar cells
ISCs
intestinal stem cells
Lgr5
Leucine-rich repeat-containing G-protein-coupled receptor 5
Parp3
Poly (ADP-ribose) polymerase 3
BrdU
5-Bromodeoxyuridinc
MMP-7
Matrix metalloproteinase-7
Olfm4
Olfactomedin-4
TUNEL
TdT-mediated dUTP Nick-End Labeling

Declarations

Acknowledgements

The authors thank prof. Andy Peng Xiang from Center for Stem Cell Biology and Tissue Engineering of Sun Yat-Sen University and Ms. Yuehan Pan from animal center of the Third Affiliated Hospital of Sun Yat-Sen University for technological support.

Author contributions

XYP participated in design of the study, carried out the experiments (staining, organoids culture, gene and protein determination), participated in the sequence alignment, collected the data and performed the statistical analysis, and drafted the manuscript. HLL managed the animals, participated in molecular genetic studies and assisted with experiments. JCW participated in design and guidance of the study and participated in the sequence alignment, and helped to draft the manuscript. JJ participated in molecular genetic studies and assisted with the experiments. HNC participated in the sequence alignment and helped to take photos. JT assisted with the experiments. BW conceived of the study, designed and guided the study, and drafted the manuscript. All authors have read and approved the final manuscript.

Funding

This work was supported by grants from the National Natural Science Foundation of China (82070574) and the Natural Science Foundation Team Project of Guangdong Province (2018B03031200).

Availability of data and materials

All relevant data and material to reproduce the findings in the manuscript are available from corresponding author.

Ethics approval and consent to participate

The animal use and experiments procedures were approved by the Ethics Committee of the Third Affiliated Hospital of Sun Yat-Sen University.

Consent for publication

Not applicable in this section.

Competing Interests

The authors declare no competing financial interests.

References

1. Chen Y, Cui W, Li X, Yang H. Interaction Between Commensal Bacteria, Immune Response and the Intestinal Barrier in Inflammatory Bowel Disease. Front Immunol. 2021 Nov 11;12:761981. doi: 10.3389/fimmu.2021.761981. PMID: 34858414; PMCID: PMC8632219.
2. Funk MC, Zhou J, Boutros M Ageing, metabolism and the intestine. EMBO Rep. 2020 Jul 3;21(7):e50047. doi: 10.15252/embr.202050047. Epub 2020 Jun 21. PMID: 32567155; PMCID: PMC7332987.
3. Adams PD, Jasper H, Rudolph KL. Aging-Induced Stem Cell Mutations as Drivers for Disease and Cancer. Cell Stem Cell. 2015 Jun 4;16(6):601-12. doi: 10.1016/j.stem.2015.05.002. PMID: 26046760; PMCID: PMC4509784.
4. Siegel RL, Miller KD, Goding Sauer A, Fedewa SA, Butterly LF, Anderson JC, Cercek A, Smith RA, Jemal A. Colorectal cancer statistics, 2020. CA Cancer J Clin. 2020 May;70(3):145-164. doi: 10.3322/caac.21601. Epub 2020 Mar 5. PMID: 32133645.
5. De Bandt JP, Waligora-Dupriet AJ, Butel MJ. Intestinal microbiota in inflammation and insulin resistance: relevance to humans. Curr Opin Clin Nutr Metab Care. 2011 Jul;14(4):334-40. doi: 10.1097/MCO.0b013e328347924a. PMID: 21587065.
6. Abenavoli L, Scarpellini E, Colica C, Boccuto L, Salehi B, Sharifi-Rad J, Aiello V, Romano B, De Lorenzo A, Izzo AA, Capasso R. Gut Microbiota and Obesity: A Role for Probiotics. Nutrients. 2019 Nov

7;11(11):2690. doi: 10.3390/nu11112690. PMID: 31703257; PMCID: PMC6893459.

7. Soenen S, Rayner CK, Jones KL, Horowitz M. The ageing gastrointestinal tract. Curr Opin Clin Nutr Metab Care. 2016;19:12–8.
8. van der Flier LG, Clevers H. Stem cells, self-renewal, and differentiation in the intestinal epithelium. Annu Rev Physiol. 2009;71:241-60. doi: 10.1146/annurev.physiol.010908.163145. PMID: 18808327.
9. Gehart H, Clevers H. Tales from the crypt: new insights into intestinal stem cells. Nat Rev Gastroenterol Hepatol. 2019 Jan;16(1):19-34. doi: 10.1038/s41575-018-0081-y. PMID: 30429586.
10. Nalapareddy K, Nattamai KJ, Kumar RS, Karns R, Wikenheiser-Brokamp KA, et al. Canonical Wnt signaling ameliorates aging of intestinal stem cells. Cell Rep. 2017;18:2608–21.
11. Pentinmikko N, Iqbal S, Mana M, Andersson S, Cognetta AB 3rd, et al. Notum produced by Paneth cells attenuates regeneration of aged intestinal epithelium. Nature. 2019;571:398–402.
12. Martin K, Potten CS, Roberts SA, Kirkwood TB. Altered stem cell regeneration in irradiated intestinal crypts of senescent mice. J Cell Sci. 1998;111(Part 16):2297–303.
13. Nalapareddy K, Choudhury AR, Gompf A, Ju Z, Ravipati S, et al. CHK2-independent induction of telomere dysfunction checkpoints in stem and progenitor cells. EMBO Rep. 11:619–25.
14. Jurk D, Wilson C, Passos JF, Oakley F, Correia-Melo C, et al. Chronic inflammation induces telomere dysfunction and accelerates ageing in mice. Nat Commun. 2014;2:4172.
15. Kléber M, Sommer L. Wnt signaling and the regulation of stem cell function. Curr Opin Cell Biol. 2004 Dec;16(6):681–7.
16. Gehart H, Clevers H. Tales from the crypt: new insights into intestinal stem cells. Nat Rev Gastroenterol Hepatol. 2019 Jan;16(1):19–34.
17. Kodandaramireddy Nalapareddy KJ, Nattamai RS, Kumar R, Karns, Kathryn A, Wikenheiser-Brokamp LL, Sampson MM, Mahe N, Sundaram M-B, Yacyshyn B, Yacyshyn MA, Helmrath. Yi Zheng, Hartmut Geiger. Canonical Wnt Signaling Ameliorates Aging of Intestinal Stem Cells, Cell Reports, Volume 18, Issue 11, 2017, Pages 2608-2621, ISSN 2211–1247.
18. Morris O, Deng H, Tam C, Jasper H. Warburg-like metabolic reprogramming in aging intestinal stem cells contributes to tissue hyperplasia. Cell Rep. 2020;33:108423.
19. Escobar KA, Cole NH, Mermier CM, VanDusseldorp TA. Autophagy and aging: Maintaining the proteome through exercise and caloric restriction. Aging Cell. 2019 Feb;18(1):e12876. doi:10.1111/acel.12876. Epub 2018 Nov 15.
20. Passos JF, Saretzki G, Ahmed S, Nelson G, Richter T, Peters H, Wappler I, Birket MJ, Harold G, Schaeuble K, et al: Mitochondrial dysfunction accounts for the stochastic heterogeneity in telomere-dependent senescence. PLoS Biol. 5:e110200.
21. Garschall K, Dellago H, Gáliková M, Schosserer M, Flatt T, Grillari J. Ubiquitous overexpression of the DNA repair factor dPrp19 reduces DNA damage and extends Drosophila life span. NPJ Aging Mech Dis. 2017 Mar 15;3:5. doi: 10.1038/s41514-017-0005-z. Erratum in: NPJ Aging Mech Dis. 2017 Aug 15;3:10.

22. Saffrey MJ. Aging of the mammalian gastrointestinal tract: a complex organ system. Age (Dordr). 2014 Jun;36(3):9603. doi:10.1007/s11357-013-9603-2. Epub 2013 Dec 20. PMID: 24352567; PMCID: PMC4082571.
23. Moorefield EC, Andres SF, Blue RE, Van Landeghem L, Mah AT, Santoro MA, Ding S. Aging effects on intestinal homeostasis associated with expansion and dysfunction of intestinal epithelial stem cells. Aging (Albany NY). 2017 Aug 29;9(8):1898-1915. doi: 10.18632/aging.101279. PMID: 28854151; PMCID: PMC5611984.
24. Nalapareddy K, Nattamai KJ, Kumar RS, Karns R, Wikenheiser-Brokamp KA, Sampson LL, Mahe MM, Sundaram N, Yacyshyn MB, Yacyshyn B, Helmrath MA, Zheng Y, Geiger H. Canonical Wnt Signaling Ameliorates Aging of Intestinal Stem Cells. Cell Rep. 2017 Mar 14;18(11):2608-2621. doi: 10.1016/j.celrep.2017.02.056. PMID: 28297666; PMCID: PMC5987258.
25. Haber AL, Biton M, Rogel N, Herbst RH, Shekhar K, Smillie C, Burgin G, Delorey TM, Howitt MR, Katz Y, Tirosh I, Beyaz S, Dionne D, Zhang M, Raychowdhury R, Garrett WS, Rozenblatt-Rosen O, Shi HN, Yilmaz O, Xavier RJ, Regev A. A single-cell survey of the small intestinal epithelium. Nature. 2017 Nov 16;551(7680):333–339. doi: 10.1038/nature24489. Epub 2017 Nov 8. PMID: 29144463; PMCID: PMC6022292.
26. Tremblay S, Côté NML, Grenier G, Duclos-Lasnier G, Fortier LC, Ilangumaran S, Menendez A. Ileal antimicrobial peptide expression is dysregulated in old age. Immun Ageing. 2017 Aug 29;14:19. doi: 10.1186/s12979-017-0101-8. PMID: 28855949; PMCID: PMC5575895.
27. Pentinmikko N, Iqbal S, Mana M, Andersson S, Cognetta AB 3rd, Suciu RM, Roper J, Luopajärvi K, Markelin E, Gopalakrishnan S, Smolander OP, Naranjo S, Saarinen T, Juuti A, Pietiläinen K, Auvinen P, Ristimäki A, Gupta N, Tammela T, Jacks T, Sabatini DM, Cravatt BF, Yilmaz ÖH, Katajisto P. Notum produced by Paneth cells attenuates regeneration of aged intestinal epithelium. Nature. 2019 Jul;571(7765):398–402. doi: 10.1038/s41586-019-1383-0. Epub 2019 Jul 10. PMID: 31292548; PMCID: PMC8151802.
28. Mahe MM, Aihara E, Schumacher MA, Zavros Y, Montrose MH, Helmrath MA, Sato T, Shroyer NF. Establishment of Gastrointestinal Epithelial Organoids. Curr Protoc Mouse Biol. 2013 Dec 19;3(4):217-40. doi: 10.1002/9780470942390.mo130179. PMID: 25105065; PMCID: PMC4120977.
29. Saffrey MJ. Aging of the mammalian gastrointestinal tract: a complex organ system. Age (Dordr). 2014 Jun;36(3):9603. doi:10.1007/s11357-013-9603-2. Epub 2013 Dec 20. PMID: 24352567; PMCID: PMC4082571.
30. Rouleau M, McDonald D, Gagné P, Ouellet ME, Droit A, Hunter JM, Dutertre S, Prigent C, Hendzel MJ, Poirier GG. PARP-3 associates with polycomb group bodies and with components of the DNA damage repair machinery. J Cell Biochem. 2007 Feb 1;100(2):385-401. doi: 10.1002/jcb.21051. PMID: 16924674.
31. Loseva O, Jemth AS, Bryant HE, Schüler H, Lehtiö L, Karlberg T, Helleday T. PARP-3 is a mono-ADP-ribosylase that activates PARP-1 in the absence of DNA. J Biol Chem. 2010 Mar 12;285(11):8054-60. doi: 10.1074/jbc.M109.077834. Epub 2010 Jan 11. PMID: 20064938; PMCID: PMC2832956.

32. Boehler C, Gauthier LR, Mortusewicz O, Biard DS, Saliou JM, Bresson A, Sanglier-Cianferani S, Smith S, Schreiber V, Boussin F, Dantzer F. Poly(ADP-ribose) polymerase 3 (PARP3), a newcomer in cellular response to DNA damage and mitotic progression. Proc Natl Acad Sci U S A. 2011 Feb 15;108(7):2783–8. doi: 10.1073/pnas.1016574108. Epub 2011 Jan 26. PMID: 21270334; PMCID: PMC3041075.
33. Day TA, Layer JV, Cleary JP, Guha S, Stevenson KE, Tivey T, Kim S, Schinzel AC, Izzo F, Doench J, Root DE, Hahn WC, Price BD, Weinstock DM. PARP3 is a promoter of chromosomal rearrangements and limits G4 DNA. Nat Commun. 2017 Apr 27;8:15110. doi: 10.1038/ncomms15110. Erratum in: Nat Commun. 2017 Jun 13;8:15918. PMID: 28447610; PMCID: PMC5414184.
34. Rodriguez-Vargas JM, Martin-Hernandez K, Wang W, Kunath N, Suganthan R, Amé JC, Oliver FJ, Ye J, Bjørås M, Dantzer F. Parp3 promotes astrocytic differentiation through a tight regulation of Nox4-induced ROS and mTorc2 activation. Cell Death Dis. 2020 Nov 6;11(11):954. doi: 10.1038/s41419-020-03167-5. PMID: 33159039; PMCID: PMC7648797.
35. Beck C, Rodriguez-Vargas JM, Boehler C, Robert I, Heyer V, Hanini N, Gauthier LR, Tissier A, Schreiber V, Elofsson M, Reina San Martin B, Dantzer F. PARP3, a new therapeutic target to alter Rictor/mTORC2 signaling and tumor progression in BRCA1-associated cancers. Cell Death Differ. 2019 Sep;26(9):1615–1630. doi: 10.1038/s41418-018-0233-1. Epub 2018 Nov 15. PMID: 30442946; PMCID: PMC6748154.
36. Sharif-Askari B, Amrein L, Aloyz R, Panasci L. PARP3 inhibitors ME0328 and olaparib potentiate vinorelbine sensitization in breast cancer cell lines. Breast Cancer Res Treat. 2018 Nov;172(1):23–32. doi:10.1007/s10549-018-4888-6. Epub 2018 Jul 23. PMID: 30039287.

Figures

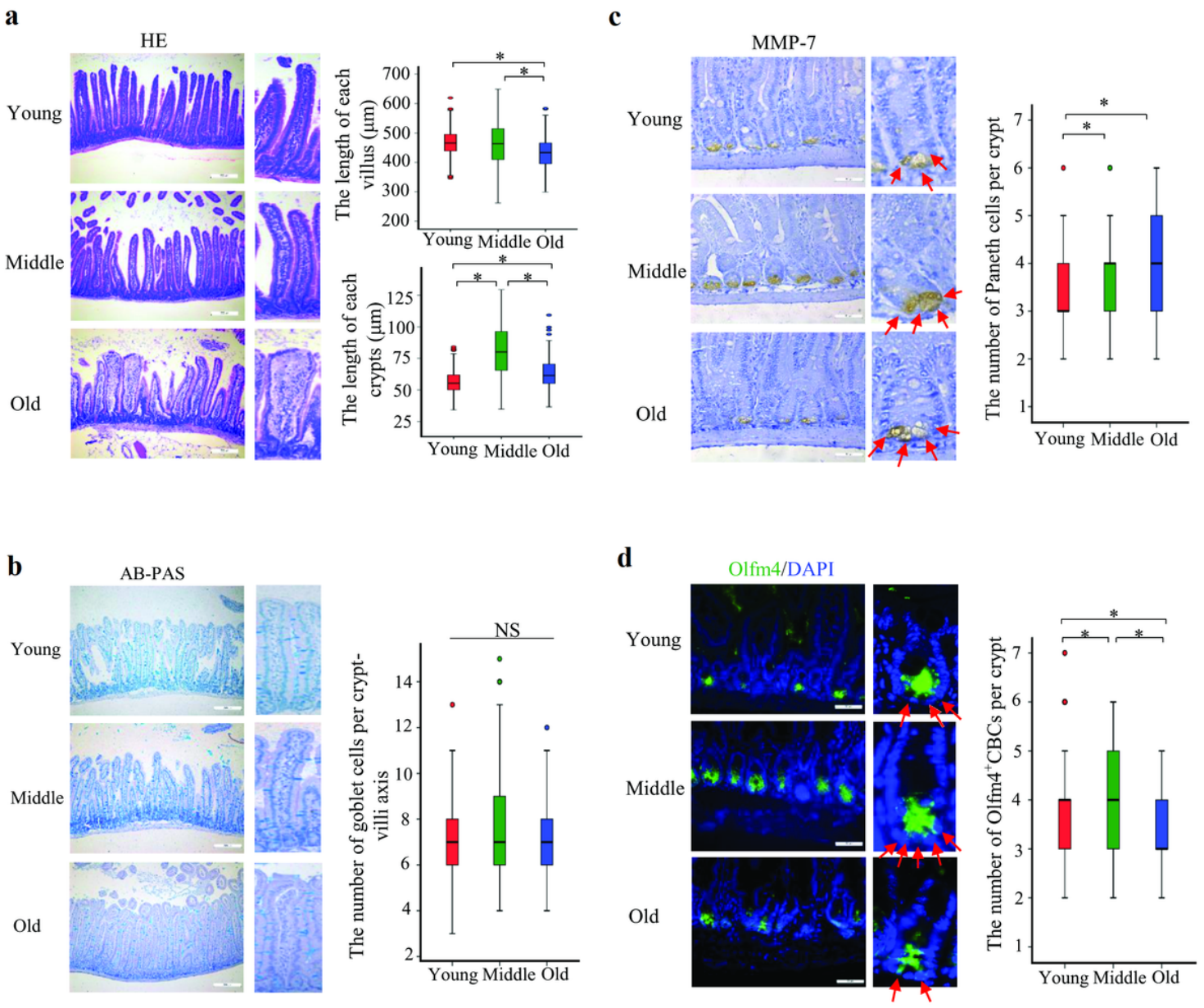

Figure 1

Intestinal villus length and crypt base columnar (CBC) were reduced in aging.

(a) The picture showed the hematoxylin-eosin staining of small intestine. The villi length and crypt depth were counted in 5 100×field each sample (30-40 units). Values are presented in box plots, n=5 in each group; *P<0.017 between two groups. (b) The goblet cells were marked by Alcian blue and Periodic Acid-Schiff staining (blue). The number of goblet cells in each crypt-villi axis was counted in 5 100×field each sample (25-30 units). Values are presented in box plots, n=5 in each group. (c) The Paneth cells were marked by MMP-7 immunohistochemistry staining (brown). The number of Paneth cells in each crypt was counted in 5 high power field (HP,400×) (25-30 units). Values are presented in box plots, n=5 in each group; *P<0.017 between two groups. (d) The intestinal stem cells (ISCs) were marked by Olfm4 immunofluorescence (green). The number of Olfm4$^+$ crypt base columnar (CBC) in each crypt was

counted in 5 HP each sample (25-30 units). Values are presented in box plots, n=5 in each group; *P<0.017 between two groups.

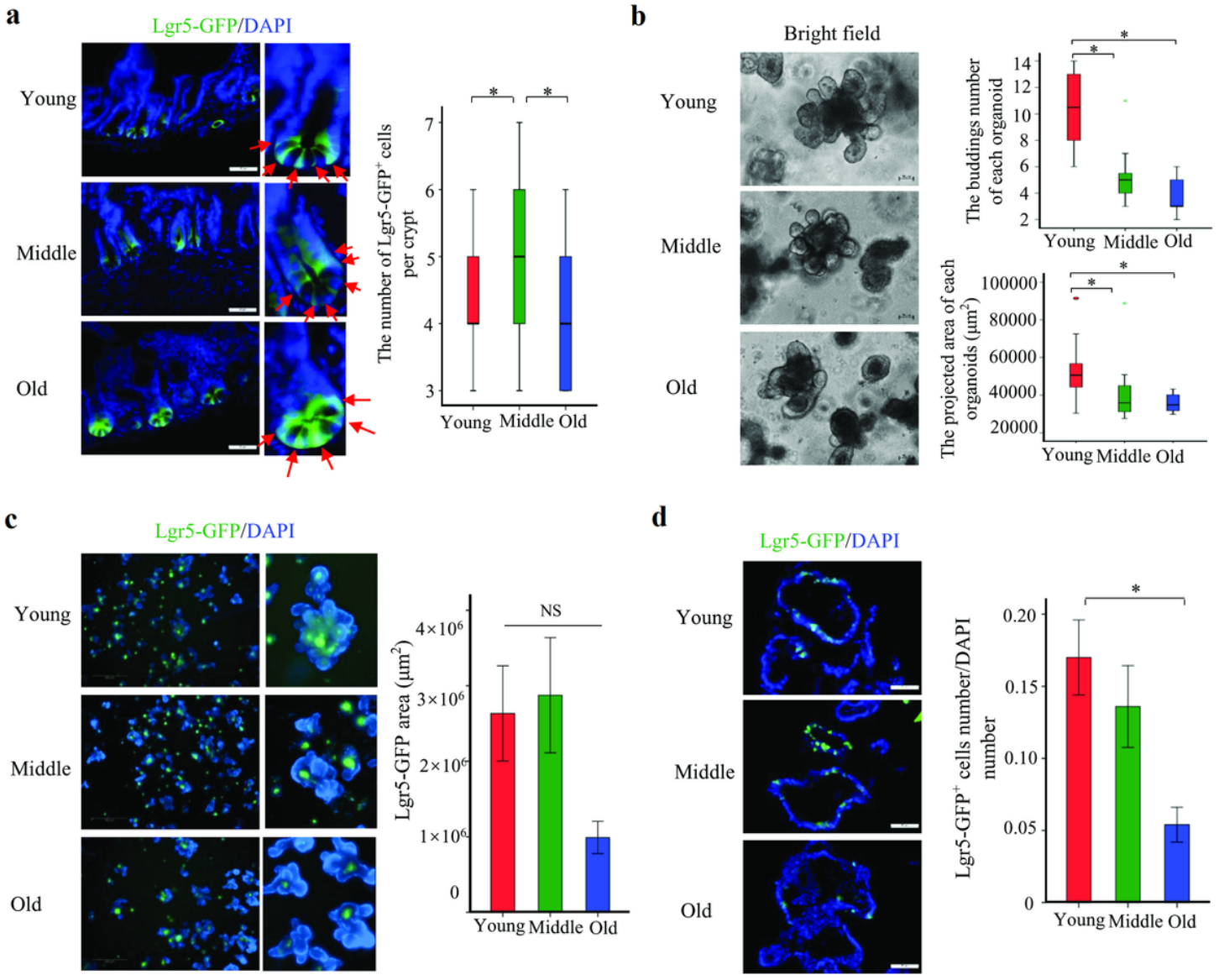

Figure 2

Lgr5$^+$ intestinal stem cells (ISCs) were reduced in aging mice and intestinal organoids.

(a) The Lgr5$^+$ISCs was marked by autofluorescence of Lgr5-eGFP knock-in transgenetic mice (green). The number of Lgr5$^+$ISCs in each crypt was counted in 5 HP (25-30 units). Values are presented in box plots, n=5 in each group; *P<0.017 between two groups. (b) The picture showed the organoids after 7 days cultured under bright field. 10 largest organoids of each group were chosen to count the buddings number and projected area. Values are presented in box plots. *P<0.017 between two groups. (c) The picture showed organoids after 7 days cultured under high-content cell analyzer. The Lgr5$^+$ISCs was marked by autofluorescence(green). The area of GFP was counted by high-content cell analyzer. Values

are means ± SE, n=8 in each group. *P*=0.067 among three groups. (d) The Lgr5^{+}ISCs was marked by autofluorescence. The number of Lgr5^{+}ISCs and number of DAPI was counted in 5 HP and their ratio was calculated. Values are means ± SE. *P<0.05 between young and old group.

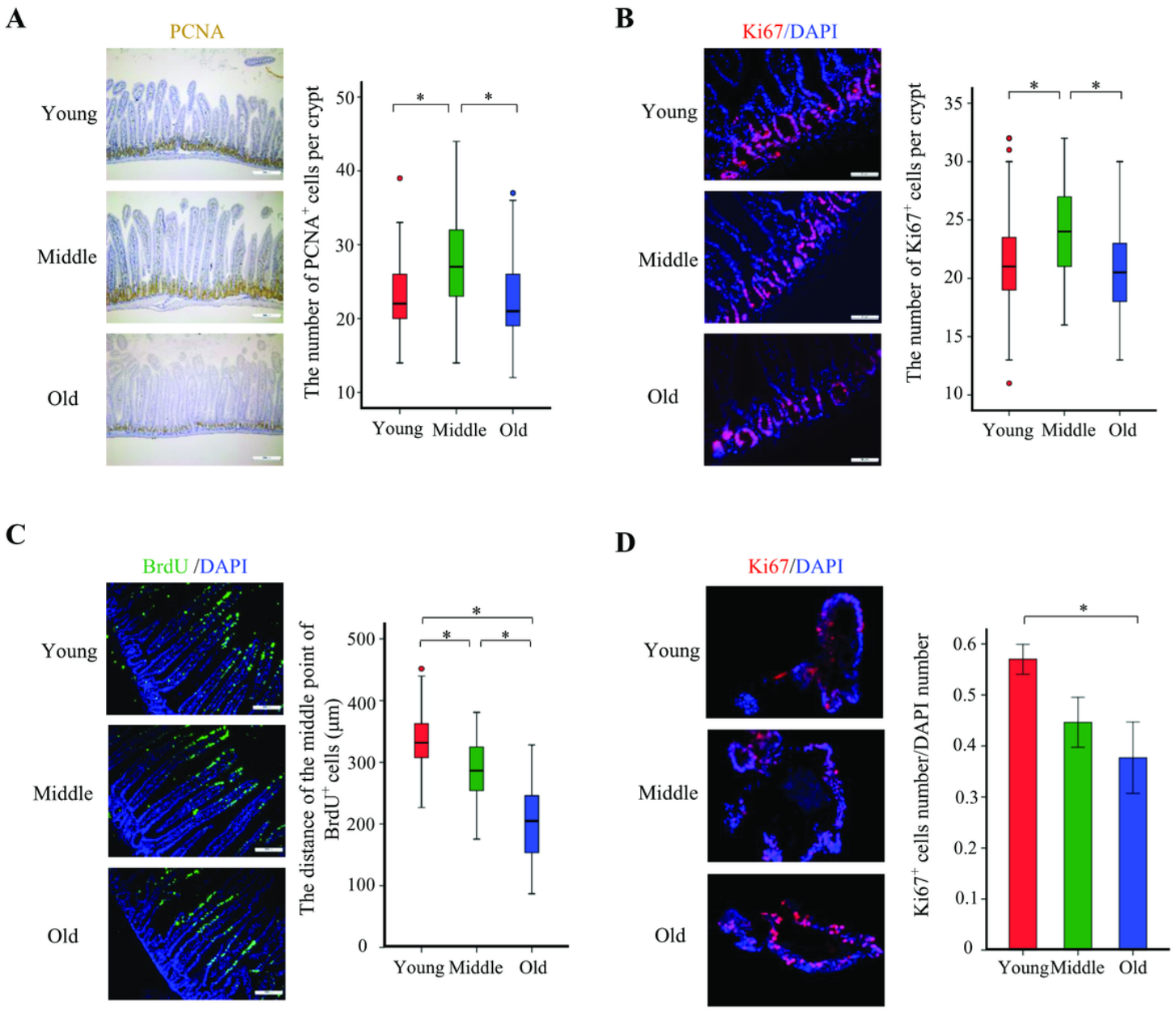

Figure 3

Intestinal cellular proliferation was downregulation in aging mice and intestinal organoids.

(a) The proliferating cells were marked by PCNA immunohistochemistry staining (brown). The number of proliferating cells in each crypt was counted in 5 HP (15-20 units). Values are presented in box plots, n=5 in each group; *P<0.017 between two groups. (b) The proliferating cells were marked by Ki67 immunofluorescence staining. (red) The number of proliferating cells in each crypt was counted in 5 HP (15-20 units). Values are presented in box plots, n=3 in each group; *P<0.017 between two groups. (c) The

wild type mice were intraperitoneal injected with 1mg/10g BrdU solution. The jejunum sample was collected after 72 hours. The BrdU was marked by BrdU immunofluorescence staining (green). The distance from the bottom of villi to the middle point of $BrdU^+$ cells was counted in 5 100×field each sample(20-30 units). Values are presented in box plots, n=3 in each group. *P<0.017 between two groups. (d) The proliferating cells in 7-day cultured organoids was marked by Ki67 immunofluorescence staining. The number of proliferating cells and number of DAPI was counted in 5 HP each group and their ratio were calculated. Values are means ± SE. *P<0.05 between young and old group.

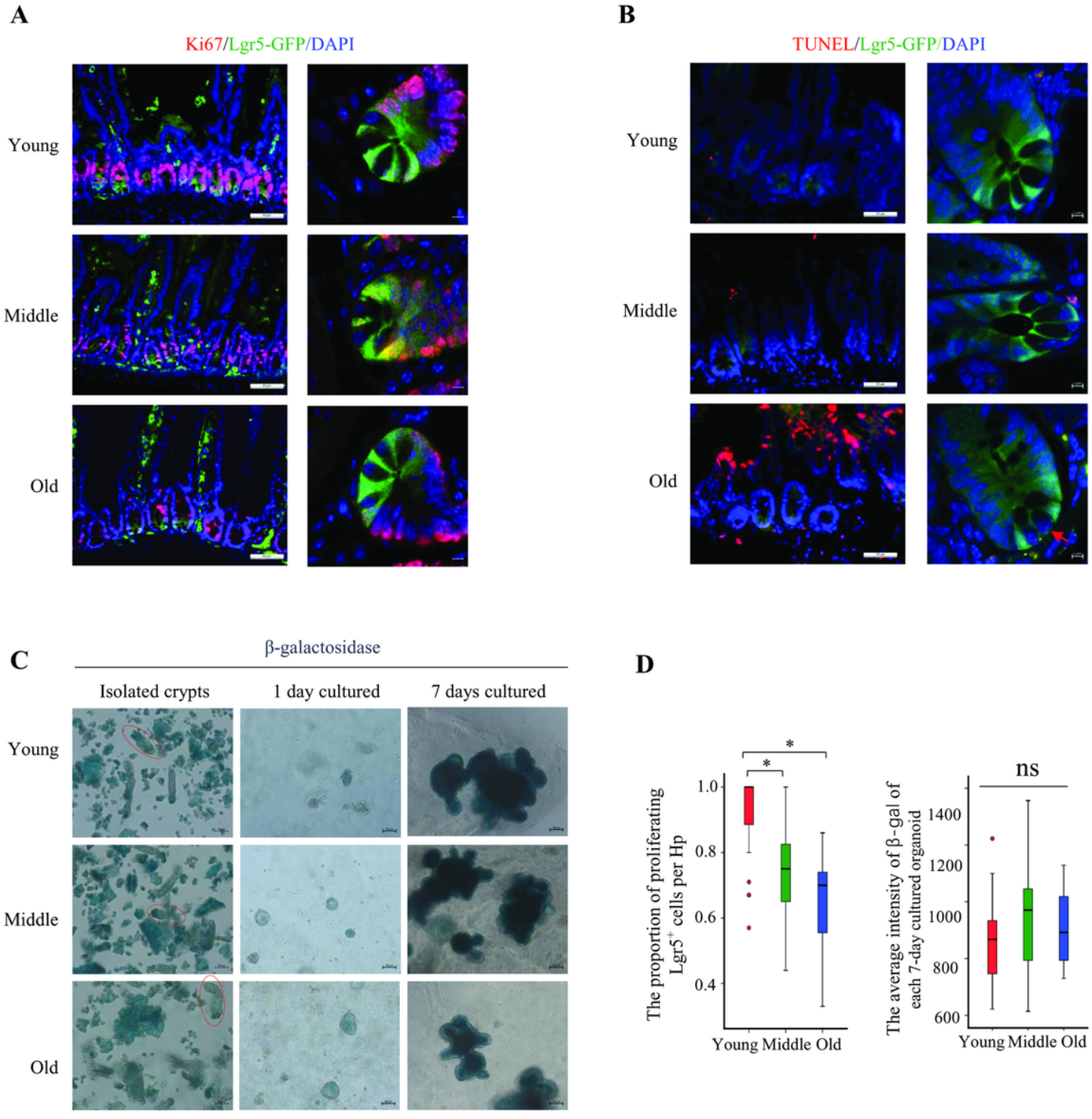

Figure 4

Proliferation of Lgr5^{+} ISCs was restrained in aging mice.

(a) The upper picture showed the double immunofluorescence staining of Ki67 (red) and Lgr5-GFP (green). The lower pictures were taken by confocal microscope. The Lgr5^{+}ISCs was marked by autofluorescence and proliferating cells was marked by Ki67 immunofluorescence staining. (b) The apoptosis cells were marked by TUNEL staining and the Lgr5^{+} ISCs was marked by autofluorescence. The lower pictures were taken by confocal microscope. (c)The senescent cells were marked by β-galactosidase staining. (blue). Red circles marked the crypts. (d) The number of proliferating Lgr5^{+}ISCs and number of Lgr5^{+}ISCs was counted in 5 HP each sample and their ratio were calculated. Values are presented in box plots, n=3 in each group. *P<0.017 between two groups. The intensity of β-gal of each 7-day cultured organoids was counted. Values are presented in box plots, n=17 in each group.

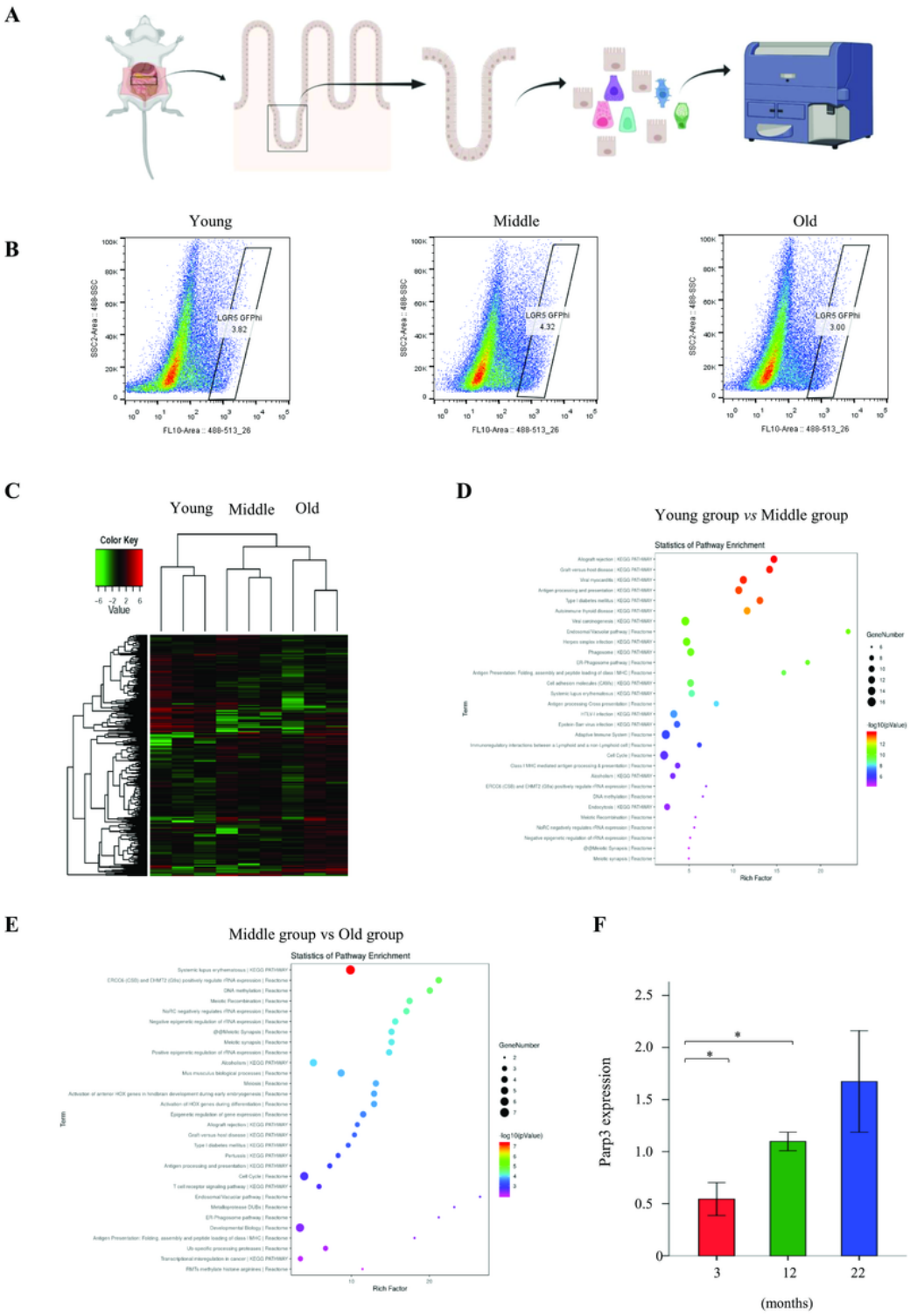

Figure 5

Parp3 gene was upregulated in intestinal Lgr5^{+} stem cells of aging mice.

(a)The picture showed the procedure of Lgr5^{+} stem cells isolation. 1/3 length of proximal small intestine was cut from Lgr5-eGFP knock-in mouse (n=3 in each group). The crypts and villi were isolated from tissue by incubated with 5mM EDTA solution. The crypts were isolated through 100μm cell filters. Then

the crypts were digested into single cells for FASC. (b) The flow chart showed the ratio of Lgr5^{hi} cells in crypt cells. The cells into the square were sorted for bulk sequence. (c) According to the gene expression, 9 samples were divided into 3 clusters. The clusters are consistent with the actual age groups. (d) The top 30 pathways with statistical significance ranked by *p* value between young group and middle group. (e) The top 30 pathways with statistical significance ranked by *p* value between middle group and old group. (f) The gene expression of Parp3. Values are mean±SE, n=3 each group.*P<0.05 between two group.

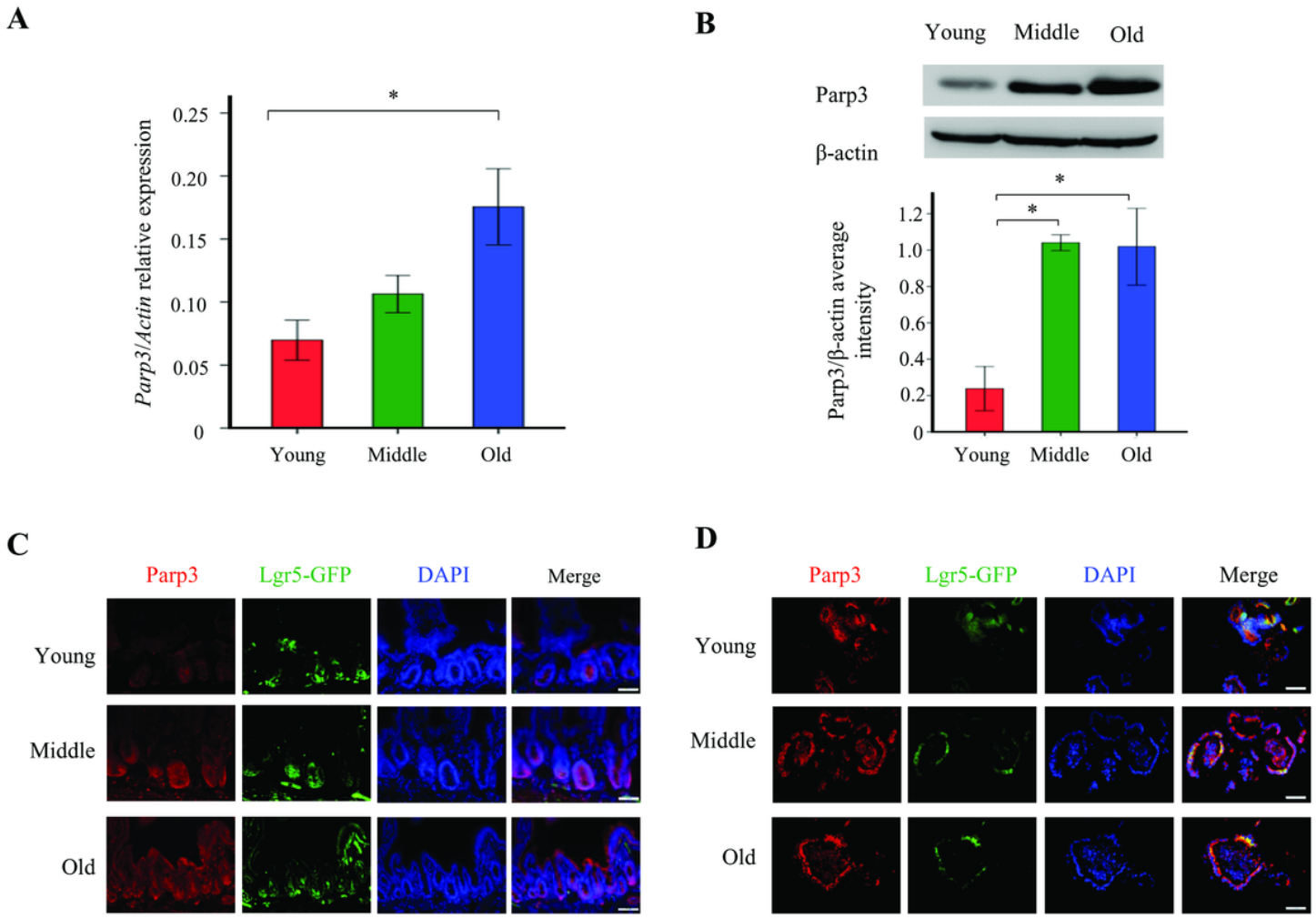

Figure 6

Parp3 was overexpressed in intestinal mucosa and intestinal organoids of aging mice.

(a) The Parp3 gene expression was determined by RT-PCR. Values are mean±SE, n=4 each group. *P<0.05 between young and old group. (b) The protein level of Parp3 was determined by western-blotting. The values are mean±SE, n=3 each group. *P<0.05 between two groups. (c)The picture showed the tissue section staining. Parp3 was marked by immunofluorescence (red) and Lgr5^{+} ISCs were marked by autofluorescence (green). (d)The picture showed the organoids section staining. Parp3 was marked by immunofluorescence (red) and Lgr5^{+} ISCs were marked by GFP immunofluorescence (green).

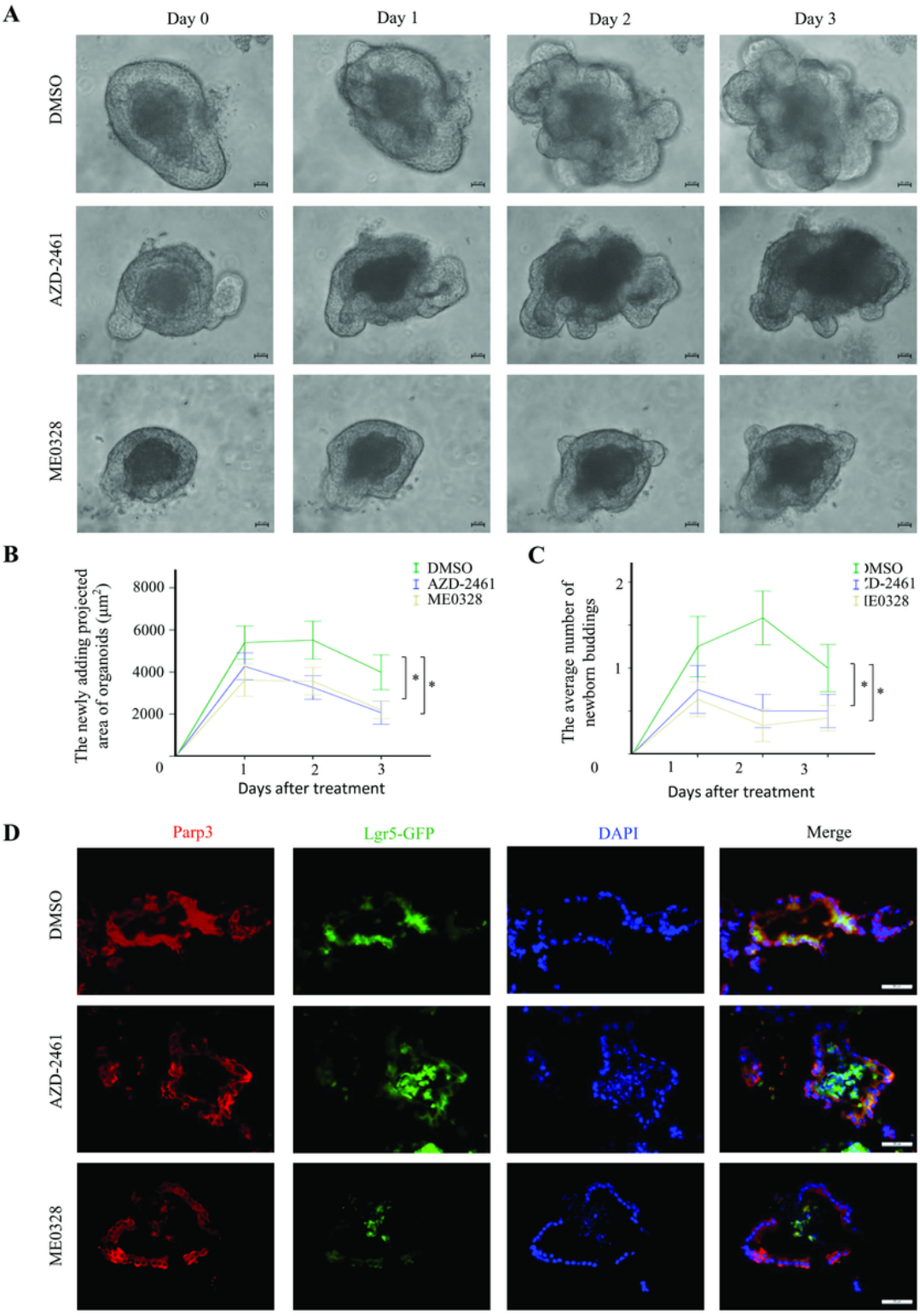

Figure 7

Inhibition of Parp3 depressed intestinal organoids growth in aging.

(a) Organoids isolated from middle age mice were after three days normal cultured. In the fourth day, Parp3 inhibition (AZD-2461 and ME0328) and DMSO were added into culture medium repeating in fifth day and sixth day. 12 organoids in each group were chosen to count the projected area and the number

of newborn buddings every day lasting from the fourth day to the seventh day. (b) The number of newborn buddings were counted every day after treatment. Values are mean±SE. The adding projected area every day was the difference value compared with former day. Values are mean±SE.*P<0.05 (c) The picture showed the organoids section staining. Parp3 was marked by immunofluorescence (red) and Lgr5$^+$ ISCs were marked by autofluorescence (green).

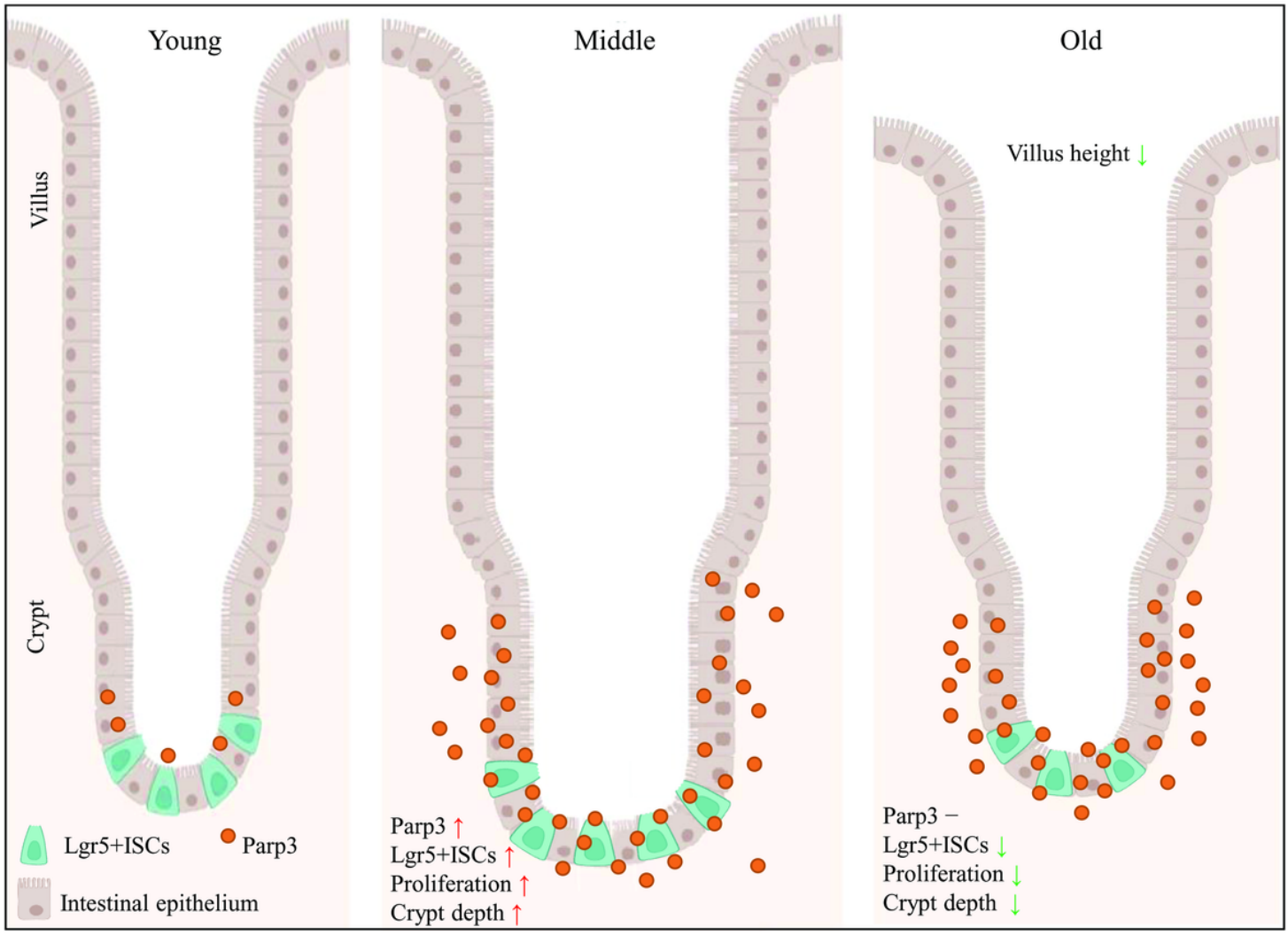

Figure 8

Lgr5$^+$ stem cells and intestinal aging

From young to middle age, the crypts depth, Lgr5$^+$ ISCs number and proliferating cells are increased which might relate to increase expression of Parp3. From middle age to old age, the level of Parp3 has no difference with middle age. The decrease of Lgr5$^+$ ISCs and proliferation cause the villi height decreased.